Spatial distribution and near-field coupling of surface plasmon polariton Bloch modes

M. Sandtke and L. Kuipers*
FOM Institute for Atomic and Molecular Physics (AMOLF), Kruislaan 407, 1098 SJ Amsterdam, The Netherlands
(Received 25 January 2008; revised manuscript received 1 April 2008; published 25 June 2008)

The Bloch nature of surface plasmon polaritons in a one-dimensional plasmonic crystal is directly observed using ultrafast and phase-sensitive near-field microscopy. Individual Bloch harmonics within one Bloch mode are separated and visualized. Different harmonics within the same Bloch mode turn out to have a different lateral amplitude distribution. The coupling between the different Bloch harmonics and a near-field probe is studied by comparing the measured energy distribution over the different harmonics to the theoretically expected distribution. It is found that higher order harmonics couple more efficiently to the probe than lower order harmonics.

DOI: 10.1103/PhysRevB.77.235439 PACS number(s): 71.38.−k, 42.70.Qs, 68.37.Uv

I. INTRODUCTION

When a wave propagates through an infinite periodic medium, its shape has to conform to the periodicity of the medium: Bloch's theorem has to be obeyed.[1] As a result, Bloch modes will form, each consisting of multiple plane waves, called Bloch harmonics. These Bloch harmonics each have their own wave vector and all these wave vectors are separated by an integer number times $2\pi/a$ (with a the period of the medium) and one harmonic will appear in each Brillouin zone of the dispersion diagram. The different harmonics form a discrete group of coherent waves, without any redistribution of energy.[2] An individual Bloch harmonic will in general not satisfy Maxwell's equations for the periodic medium and therefore cannot exist on its own.

The influence of a periodic potential on waves is ubiquitous in many aspects of physics and examples range from electrons[3] and phonons[4,5] in atomic lattices, photons in photonic crystals,[6] or optically induced lattices[7] to, recently, surface plasmon polaritons (SPPs) in plasmonic crystals.[8] Studying Bloch modes will provide insight in the dispersion of the periodic crystal structures for electromagnetic waves and reveals, e.g., group and phase velocities. Also the ratio between the amplitudes of the different harmonics provides an elegant way of determining extremely small variations in the refractive index due to the periodic potential of the crystal.[9] A way to investigate Bloch modes in optical systems is by looking at scattered photons in the far field, e.g., with a "conventional" optical microscope.[10] However, this method relies on imperfections in the structure to scatter the photons from their bound mode to radiative modes that can be detected in the far field. In addition, a microscope in the far field is governed by diffraction which limits the spatial resolution. For photons inside a photonic crystal waveguide, a photon scanning tunneling microscope (PSTM) has been used to resolve the different photonic Bloch modes and separate the Bloch harmonics comprising each Bloch mode.[6,11,12] The individual Bloch harmonics in the photonic crystal waveguide turned out to have different lateral mode profiles.[6] A similar in depth investigation of plasmonic Bloch modes is lacking.

In this paper we investigate surface plasmon polaritons in a plasmonic crystal to study their Bloch nature. With a phase-sensitive near-field microscope we visualize the different Bloch harmonics that build up one plasmonic Bloch mode. We show that if any dynamic interplay of the harmonics belonging to a single Bloch mode occurs, it does so on a time scale smaller than 20 fs. By comparing the experimental results to the analytically calculated energy distribution over the different harmonics, we were able to extract the relative coupling efficiency of the different harmonics to the near-field probe. Since higher order harmonics have a wave vector that is larger in magnitude, the effective wavelength of the harmonic will be smaller than the near-field probe aperture, causing significant changes in the coupling efficiency between the Bloch harmonic and the near-field probe.

II. EXPERIMENTAL ASPECTS

An SPP crystal[13] was used in this study as a model structure. SPPs are the solution of Maxwell's equations at the interface between a dielectric and a metal. An SPP is a bound and propagating surface wave.[14–16] SPPs are excited on a Au-air interface with light from a Ti:sapphire laser pumped optical parametric oscillator (pulse duration of 120 fs, repetition rate of 80 MHz, wavelength tunable between 1400 and 1600 nm, and bandwidth of 30 nm). Figure 1(a) shows an optical microscopy picture of the SPP crystal. It consists of a

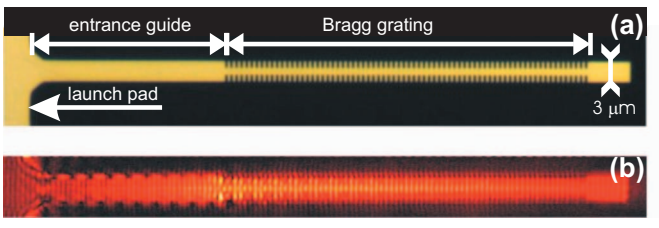

FIG. 1. (Color) (a) Optical microscope picture of the SPP grating under investigation. SPPs are excited at the launch pad at the left of the figure. They propagate via an entrance guide to a 55 μm long Bragg grating. The Bragg grating consists of periodic indentations of 1 μm (period 750 nm) leaving a 1 μm Au strip at the center. (b) Typical experimentally measured snapshot of the amplitude of the SPP field as obtained with the time-sensitive and phase-resolved PSTM. SPPs were excited with 120 fs pulses with a central wavelength in air of 1500 nm.

55 nm thick Au film on BK7 glass and is prepared by e-beam lithography and lift-off. At the left of the figure a launch pad is visible on which the SPPs are excited using a Kretschmann-Raether configuration.[17] Via a tapered entrance, SPPs are guided by a 3 μm wide entrance guide of 30 μm long to a 55 μm long Bragg grating which is created along the straight guide. The Bragg grating consists of an arrangement of 1 μm indentations with a period of 750 ± 15 nm, thus leaving a 1 μm Au strip remaining at the center. After the Bragg grating, 6 μm of unperturbed straight waveguide is continued.

We used a home-built PSTM working with shear-force height feedback, incorporated in a Mach-Zehnder-type interferometer to study the SPP Bloch behavior.[18] Acousto-optical modulators in one of the branches of the interferometer combined with a lock-in detector enable phase-sensitive measurements.[19] Raster scanning the near-field probe over the SPP grating yields information on the amplitude distribution of the E-field distribution along the grating. In addition, the signal yields the local phase evolution of the SPP E field. An optical delay line is added in the so-called reference branch of the interferometer. In this study 120 fs pulses are used to excite the SPPs. Interference between the wave packets inside the two interferometer branches will only be detected when there is temporal overlap between the wave packets at the detector. In effect the near-field microscope will measure the cross correlation between the SPP wave packet and the wave packet in the reference branch. By varying the delay line in the reference branch, interference will occur for different probe positions along the structure. For every delay line position, a different cross correlation, which resembles a snapshot of the SPP wave packet in time, is obtained. This way the dynamics of the SPPs can be studied. More detail on this instrument can be found in Ref. 18.

III. FOURIER ANALYSIS

The structure under investigation is periodic in the propagation direction (x direction) and acts as a waveguide in the direction perpendicular to this (y direction). The general expression for a single infinitely extending Bloch mode at time t and position (x,y) is therefore given by[3]

$$E(x,y,t) = \sum_m C_m(k_x,y)\exp\left[i\left(\left\{k_x + \frac{2\pi m}{a}\right\}r - \omega t\right)\right]. \quad (1)$$

Here m is an integer labeling the harmonic, ω is the angular frequency, k_x is the fundamental wave vector in the x direction, a is the grating period, and $C_m(k_x,y)$ is the complex amplitude of each Bloch harmonic. The lateral mode profile, i.e., the amplitude profile in the y direction, can be different for each Bloch harmonic, which is reflected in the explicit dependence of C_m on y. We use a two-dimensional (2D) fast Fourier transform (FFT) to obtain the different in-plane spatial frequencies present in the SPP field,[4,5]

$$F(\mathbf{k},\omega) = \frac{1}{(2\pi)^2}\int\int_{-\infty}^{+\infty} E(\mathbf{r},t)\exp[i(-\mathbf{k}\cdot\mathbf{r})]d^2\mathbf{r}. \quad (2)$$

The various peaks in the spectrum along the x direction will identify all the Bloch harmonics present. The spatial frequencies along the y direction for each of these peaks yield insight into the lateral mode profiles of each Bloch harmonic. Please note that a series of one-dimensional Fourier transforms of lines parallel to the propagation direction would, in principle, yield the same information. The two-dimensional Fourier transform was chosen for reasons of simplicity only.

Because the E field is detected by a near-field probe we have to consider that the detection efficiency for each Bloch harmonic may depend both on m and on k_x, which together determine the magnitude of the wave vector of the Bloch harmonic. For photonic systems differences in the magnitude of the wave vector can cause a change in coupling to the probe for different harmonics[20] and must therefore be taken into account. We define the detection efficiency $A_m(k_x)$ for each Bloch harmonic as follows:

$$F_m(k_x) = A_m(k_x)C_m(k_x), \quad (3)$$

where $C_m(k_x) = \int_{-\infty}^{+\infty} C_m(k_x,y)dy$ and $F_m(k_x)$ is the Fourier amplitude at $k = k_x + 2m\pi/a$ integrated for all k_y. It turns out that in the experiments that will follow, we only excite one Bloch mode at a time. This Bloch mode is composed of several Bloch harmonics.

IV. EXPERIMENTAL RESULTS

For the measurements we raster scan the near-field probe over the Bragg grating while keeping the delay time, as determined by the length of the reference branch, fixed. This method results in a typical snapshot of the propagating SPP, as is shown in Fig. 1(b). In the figure we only depict the amplitude information of the SPP field. The phase information, which is obtained simultaneously, is not shown. Already it is visible that the optical field above the grating has a periodic modulation, parallel to the propagation direction (from left to right). The observed periodicity is 750 nm, which is equal to the grating period. We therefore observe that the SPP field conforms to the grating period and forms a Bloch wave. In the entrance guide a standing-wave pattern is visible, due to reflections at the transition between the entrance guide and the grating.

A. Separating reflected surface plasmon polaritons and Bloch harmonics

By carrying out the Fourier transformation only on a selected part of the real-space data, we obtain the spatial frequencies of the selected scan area only. Figure 2 shows the result of a 2D FFT of the entrance guide for a central excitation wavelength of 1500 nm. The 2D amplitude and phase data are summed after the FFT in the direction perpendicular to the propagation direction. The peak around 4.2×10^{-3} nm^{-1} corresponds to the SPPs propagating in the entrance waveguide toward the grating. The peak around -4.2×10^{-3} nm^{-1} (indicated by an arrow) corresponds to the SPPs that have been reflected at the transition of the entrance guide and the grating. These SPPs have a negative phase velocity, since their wave vector is negative. The measured magnitude of the wave vector of the SPPs is a factor 1.01 higher than that of photons with a wavelength of 1500 nm in

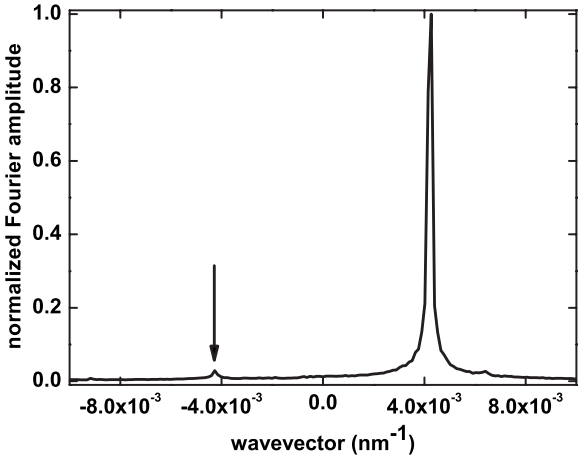

FIG. 2. Amplitude of the sum of the 2D spatial FFT of the entrance guide in the direction perpendicular to the grating, normalized to the maximum amplitude value. Around 4.2×10^{-3} nm^{-1} the SPPs propagating from left to right in Fig. 1(b) appear. The SPPs reflected at the interface between the entrance guide and grating have a negative group and phase velocity and appear at -4.2×10^{-3} nm^{-1}, indicated by the arrow.

air. This does mean that the SPPs in the waveguide have a strong photonlike character. However, they are still bound since the magnitude of their wave vector is larger than that of photons in air at the same frequency (their dispersion curve lies below the so-called lightline). The sign of the group velocity of the SPPs at -4.2×10^{-3} nm^{-1} turns out to be negative if we follow the propagation direction of the mode in time. Since these SPPs propagate in the opposite direction with respect to the initially excited SPP, we know that they have to be reflected. Interference between the two opposite propagating SPP wave packets causes the standing-wave pattern visible in the entrance guide in Fig. 1(b). The ratio between the peaks at 4.2×10^{-3} and -4.2×10^{-3} nm^{-1} gives the amplitude reflection coefficient, which is $7\%\pm2\%$.

Next we select only the fields detected along the uncorrugated central part of the Bragg structure. In first instance we do not consider the measured SPP field above the grating to avoid topographical artifacts.[21] The absolute value of the 2D FFT of the SPP amplitude in this section is shown in Fig. 3, again for an excitation wavelength of 1500 nm in air and summed after the FFT in the direction perpendicular to the propagation direction. Multiple peaks appear, representing individual Bloch harmonics, separated by $2\pi/a$: $-3\pi/a+\epsilon$ (indicated by an arrow), $-\pi/a+\epsilon$, $\pi/a+\epsilon$, and $3\pi/a+\epsilon$, with $\epsilon=0.015\times10^{-3}$ nm^{-1} for this frequency. Repeating this experiment for different frequencies results in the complete band structure of the grating (not shown in this paper), such as the band structure for photons in a photonic crystal waveguide.[6] The sign of the group velocity of the different harmonics, $\partial\omega/\partial k$, can be determined by following their propagation in time. All harmonics turn out to have a positive group velocity and are thus part of the same Bloch mode.

The observation that the SPP wave vector is very close to the wave vector of photons in air at the same frequency, combined with the finite length of the grating (55 μm),

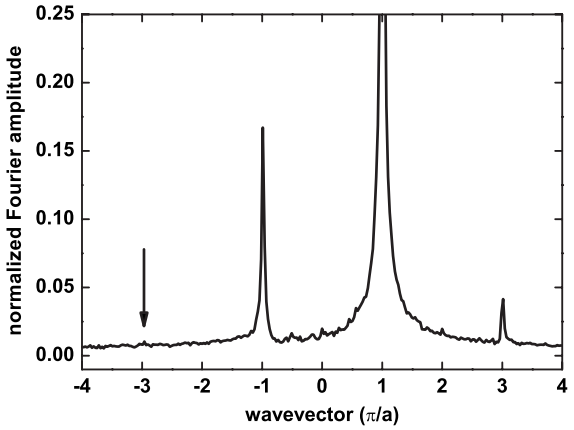

FIG. 3. Absolute value of the 2D spatial FFT of the amplitude of the SPP E-field guide in between the grating, normalized to the amplitude at π/a. Close to π/a the fundamental mode is visible and close to $-3\pi/a$ (indicated by the arrow), $-\pi/a$, and $3\pi/a$ the Bloch harmonics appear.

which results in a finite resolution of the FFT analysis of 1.1×10^{-4} nm^{-1}, has implications for the analysis of the results. The $m=-1$ Bloch harmonic and reflection of the $m=0$ harmonic at the end of the grating will both end up at the same position in the 2D FFT, i.e., at roughly $-\pi/a=-4.2\times10^{-3}$ nm^{-1}. Easy separation is only possible at frequencies for which $|k_x|\neq\pi/a\pm1.1\times10^{-4}$ nm^{-1}. At such frequencies our phase-sensitive microscope will yield two distinguishable peaks. Figure 4 shows that for an excitation wavelength in air of 1600 nm this is indeed the case. The peak at the left is the $m=1$ Bloch harmonic and the peak on the right is SPPs reflected at the end of the grating. We are able to discriminate the two by looking at their group velocity.

Since in this study we focus on the behavior of the Bloch harmonic and not on the reflected SPPs, the amplitude of the Fourier peaks around $k_x=-\pi/a$ should be corrected for the reflected SPPs to arrive at the detected signal of the $m=-1$ Bloch harmonic. Averaging over multiple measurements, all

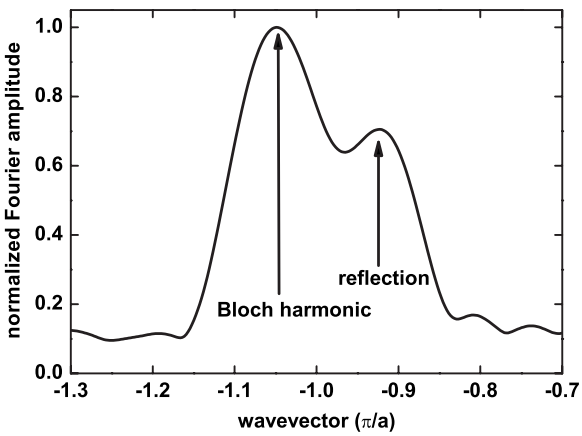

FIG. 4. FTT amplitude around $-\pi/a$, normalized to the maximum of the spectrum. At an excitation wavelength of 1600 nm the $m=-1$ Bloch harmonic and the reflected SPPs are distinguishable. The peak at the left is the Bloch harmonic and the peak on the right is the reflection.

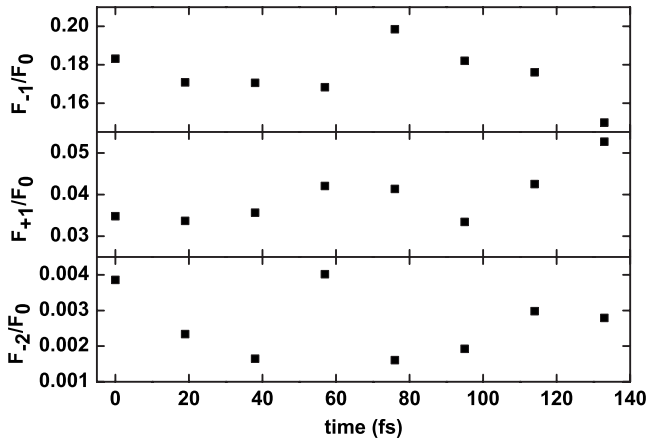

FIG. 5. Values of $F_m(k_x)$, normalized with respect to $F_0(k_x)$, for different time steps of the delay line. No clear trend is observable for any F_m. On the time scales in the experiment, Bloch harmonics do not exhibit dynamic interplay.

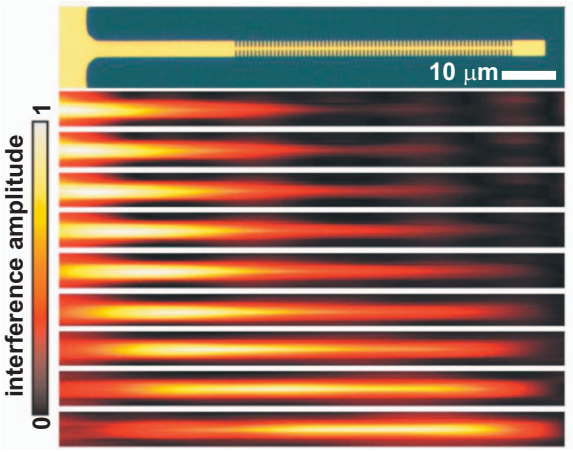

FIG. 6. (Color) In the top panel the topography of the sample is shown. In the frames below the evolution of the $m=0$ Bloch harmonic and the SPPs in the entrance guide in real space. Time between two frames is 17 fs, time progresses in the sequence of frames from top to bottom. The excitation wavelength of the SPP wave packet is 1500 nm. The colors are normalized to the maximum value in each frame. Above the entrance guide already signal is observable which is the fundamental SPP wave packet having the same wave vector as the Bloch harmonic. Along the grating the $m=0$ Bloch harmonic has a maximum above the guide in between the corrugations and it moves in time along the grating from left to right.

with different delay line positions, gives a ratio $F_{-1}/r=5.5$, with r being the amplitude of the reflected SPPs. F_{-1} and r are determined by taking the peak value of the two individual peaks. This procedure turns out to give the same results as fitting two Gaussians to the graphs like the one presented in Fig. 4. If we assume this ratio to be independent of frequency, at all frequencies, $F_{-1}=\Im(k_x)/(1+\frac{1}{5.5})=\Im(k_x)/1.18$, with $\Im(k_x)$ the total FFT amplitude found at $-\pi/a$. Once the Bloch harmonic and the reflection are separated, it is possible to determine the amplitude reflection coefficient of the end of the grating. This reflection coefficient is $4\% \pm 1\%$. When we assume that all Bloch harmonics will experience the same reflection, the amplitude of the reflection of the $m=+1$ harmonic would be 1 order of magnitude smaller than the amplitude of the Fourier peak at the position of the $m=-2$ harmonic, which will have roughly the same wave vector as the reflection of the $m=+1$ harmonic. Since the reflection of the $m=+1$ harmonic is also not visible in Fig. 4, we can and will neglect the reflections of the Bloch harmonics with $m \neq 0$.

$F_m(k_x)$ is determined for different reference times, i.e., for different positions of the SPP wave packet along the guide. The result is depicted in Fig. 5. The figure contains the relative values of $F_m(k_x)$, normalized to $F_0(k_x)$. No clear trend in time is observed for any of the Bloch harmonics. The observed fluctuations of $F_m(k_x)$ in time are comparable to the experimental uncertainty (see Fig. 8) and can be attributed to small temperature drifts and/or mechanical vibrations. The absence of a trend in Fig. 5 means that as the Bloch mode is excited, all energy within the mode is distributed over the different harmonics on a time scale below 20 fs. This observation is in agreement with predictions by Russell,[2] who stated that Bloch harmonics propagate as a unity without any redistribution of energy. We can therefore take $F_m(k_x)$, $C_m(k_x)$, and $A_m(k_x)$ to be constant in time in the rest of this investigation. All values of $F_m(k_x)$, $C_m(k_x)$, and $A_m(k_x)$ in the remainder of this paper will be the average of values obtained at different time steps to enhance statistics.

B. Mode profile of different harmonics

By Fourier analysis and filtering of the optical information, details of the spatial distribution of the individual Bloch harmonics have been obtained. Hereto, the full 2D Fourier transform is multiplied with a window function (width of $0.2\pi/a$) containing only one harmonic. Transforming the result back to real space reveals the spatial distribution of that single Bloch harmonic in two dimensions. This way it is possible to study differences in mode profile of the different harmonics, which has previously been shown for photonic Bloch harmonics.[6] However, by including the available time information we can investigate the evolution of the different harmonics in time. Selecting only the harmonic close to $+\pi/a$, or $m=0$, and Fourier transforming this back to real space reveals the evolution of the fundamental harmonic, as shown in Fig. 6. For the chosen frequency and considering the low interaction strength of the grating, the wave vector of the SPP mode in the entrance guide turns out to be equal to the wave vector of the $m=0$ harmonic of the Bloch mode in the grating. For the measurements an excitation wavelength of 1500 nm is used and the time between two frames is 17 fs. Colors are normalized to the maximum in each frame. In the top panel the topography of the grating is depicted. Comparing the different measurement frames in this figure to the frame shown in Fig. 1(b), the first thing to notice is the absence of fringes, which would have been indicative of interference effects. The standing-wave pattern in the entrance guide is no longer visible because the reflected SPPs are filtered out, this way, only the SPPs with a positive phase velocity are left. Also the amplitude modulation with a periodicity equal to the grating period in the section containing

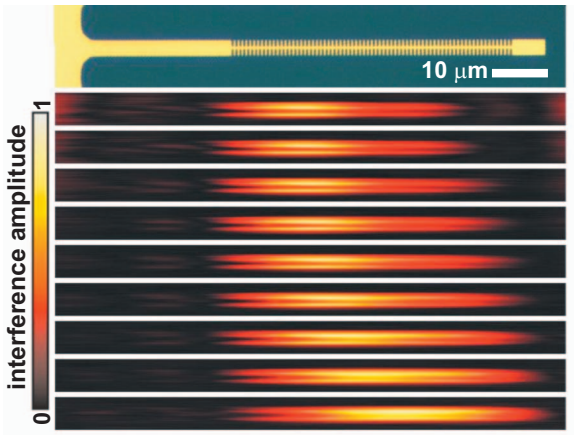

FIG. 7. (Color) In the top panel the topography of the sample is shown. In the frames below the evolution of the $m=+1$ Bloch harmonic and the SPPs in the entrance guide in real space. Time between two frames is 17 fs, time progresses in the sequence of frames from top to bottom. The first frame corresponds to the same time as the first frame in Fig. 6, same for all successive frames. The excitation wavelength of the SPP wave packet is 1500 nm. The colors are normalized to the maximum value in each frame. This harmonic has its maximum in amplitude above the corrugations and propagates from left to right as part of the Bloch mode propagating in that direction.

the grating has vanished as the periodic amplitude modulation requires the coherent superposition of two or more Bloch harmonics.

As a comparison, Fig. 7 shows the evolution of the $m=+1$ Bloch harmonic in time as obtained from the same measurement that yielded Fig. 6. The time between two successive frames is 17 fs and the excitation wavelength is 1500 nm. Because the data in Fig. 7 are obtained in the same measurement as the data shown in Fig. 6, all frames from top to bottom in Figs. 6 and 7 are measured for the same settings of the delay line. It appears as if the $m=1$ harmonic in the first time frames has propagated further into the structure than the $m=0$ harmonic. However, the apparent lead of the $m=+1$ harmonic is a consequence of the normalization to the maximum intensity within each measurement frame. The $m=+1$ harmonic is only present above the grating, and the guide in the middle of the grating, but is absent above the entrance guide. Its lateral mode profile does not change in time and has maxima above the grating. This is in contrast to the $m=0$ harmonic which has its maximum above the guide. Also the mode seems to be slightly asymmetric in the direction perpendicular to the propagation direction. We observe a slightly higher amplitude in the upper half of each frame than in the lower half. This small symmetry breaking may be explained by a small tilt of the near-field probe with respect to the sample surface.

C. $F(k_x)$ for the different harmonics

Repeating the experiments described above for different excitation wavelengths yields $F_m(k_x)$ for different wave vectors. For every excitation wavelength measurements are performed for multiple time steps. As is visible in Fig. 5, the relative strength of the different harmonics does not vary in time and therefore collecting information from multiple time frames can be used to enhance the signal-to-noise ratio. Figure 8 shows $F_m(k_x)$ for different excitation wavelengths of the Bloch mode, normalized to $F_0(k_x)$. The excitation wavelength is converted to k_x. The error bars are based on the experimental signal to noise ratio and take into account an averaging over up to five frames. The values of $F(k_x=-4.2\times10^{-3})$ are corrected for reflections of the fundamental Bloch harmonic as has been explained in Sec. IV A, which yields $F_{-1}(k_x)$. From symmetry arguments it is expected that $m=-1$ and $m=+1$ are equal, which is not the case in the measurements, as can be seen in Fig. 8. Apparently, our tip is more sensitive to harmonic $m=-1$ likely because of a small tilt of the probe. Also the $m=-2$ and $m=+2$ are not symmetric, as $m=-2$ is measurable and $m=+2$ is not. The $m=-2$ peak is 1 order of magnitude smaller than the $m=-1$ and $m=+1$ harmonics. It is important to realize here that the absolute value of the $m=-1$ and $m=+1$ harmonics is different.

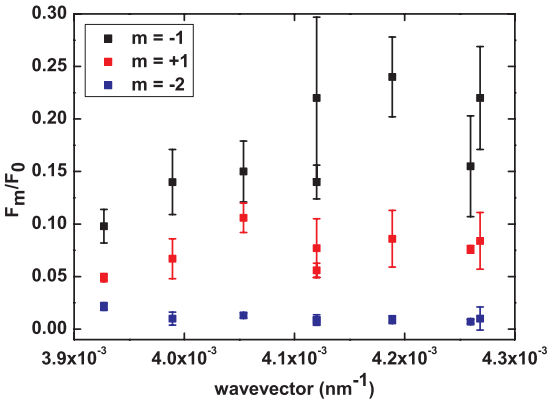

FIG. 8. (Color) $F_m(k_x)$ of the different Bloch harmonics normalized to harmonic $n=0$ for different excitation wavelengths (expressed as the wave vector of the fundamental Bloch harmonic). The error bars are the standard deviation coming from averaging over multiple time frames (typically 4).

V. THEORETICAL VALUES OF HARMONIC STRENGTH

Given the measured $F_m(k_x)$, it is possible to extract $A_m(k_x)$ once calculated values of $C_m(k_x)$ are known. To calculate $C_m(k_x)$ we use a model proposed by Russell[2] for photonic crystals. For this coupled-wave model we assume an effective dielectric constant of the periodic medium,

$$\epsilon = \epsilon_0\{1 + M\cos[(2\pi/a)x]\}, \tag{4}$$

where ϵ_0 is the effective, average value of the dielectric constant of the waveguide mode and M the modulation depth. Since we know from the experiments that losses do not prevent the Bloch mode to form along the entire grating, loss is disregarded. Note that if M goes to zero, i.e., we are left with an unperturbed waveguide, only the fundamental, $m=0$, spatial harmonic will remain and we are left with an ordinary plane wave in the waveguide. We know from experiments presented elsewhere[22] that $M=30\ \text{mm}^{-1}$ for our SPP grating.

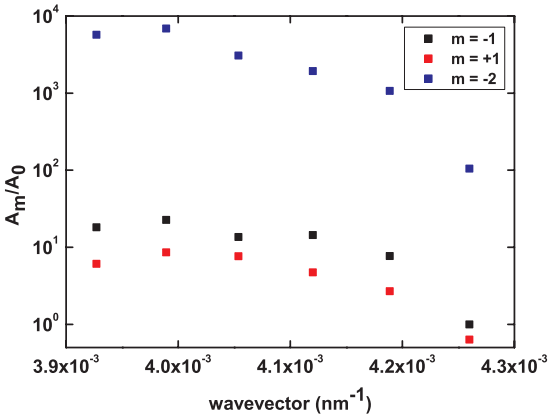

FIG. 9. (Color) $A_m(k_x)$ for the Bloch harmonics $m=1$, $m=-1$, and $m=-2$, normalized to harmonic $m=0$.

The simplest self-sufficient electromagnetic wave that can exist in such a medium is the Bloch wave as was given in Eq. (1). From the coupled-wave model it follows that the modulation strength M and optical frequency, contained in k_x, determine $C_m(k_x)$.

Substituting Eqs. (1) and (4) into the one-dimensional scalar wave equation[23] gives

$$[k^2 - (k_x + 2m\pi/a)^2]C_m(k_x) + (M/2)k^2[C_{m-1}(k_x) + C_{m+1}(k_x)] = 0, \quad (5)$$

in which $k=\omega/v_\phi$, where v_ϕ is the average phase velocity of light in the grating. In the experiment values larger than $-3\pi/a < k_x + 2m\pi/a < 3\pi/a$ are not observed. We therefore limit calculations to $-2 \leq m \leq +1$. The resulting system of linear equations can be solved with respect to an arbitrary $C_{-2}(k_x)$. Solving the equations and normalizing to the $m=0$ harmonic yields the normalized values for $C_m(k_x)$.

VI. DIFFERENT COUPLING EFFICIENCIES FOR DIFFERENT HARMONICS

Since we only know relative values for $F_m(k_x)$ and calculate only the relative values for $C_m(k_x)$, it is impossible to set absolute values to $A_m(k_x)$. Therefore we determine the value of $A_m(k_x)/A_0(k_x)$, which reflects the relative coupling efficiency for the different harmonics. Figure 9 depicts the relative coupling efficiency for different excitation wavelengths. It is clear that $A_m(k_x)/A_0(k_x)$ depends both on m and excitation wavelength. The figure shows that harmonics $m=-1$ and $m=+1$ couple five times up to 1 order of magnitude better to the probe than $m=0$ for wave vectors up to $k_x=4.5\times10^{-3}$ nm^{-1}. The coupling of the $m=-2$ harmonic for low wave vectors is 4 orders of magnitude higher than for the $m=0$ harmonic, and for larger wave vectors the ratio decreases by 2 orders of magnitude.

The difference in coupling efficiency can be understood by realizing that the different Bloch harmonics have a different wave vector. Different wave vectors may couple differently to the near-field probe as was shown for photons in Ref. 20. A larger wave vector corresponds to a smaller effective wavelength and therefore a different interaction to the subwavelength near-field probe. The difference between $m=1$ and $m=-1$ is surprising. As noted before, the harmonics do not have the same absolute wave vector. However, the $m=-1$ harmonic has a smaller absolute wave vector than the $m=+1$ harmonic, which would result in a less efficient coupling to the probe. We suspect that the difference is caused by the orientation of the probe with respect to the sample. It is possible that the probe was tilted slightly. This tilt could have resulted in the situation in which harmonics with a negative wave vector are directed toward the probe, whereas for harmonics with a positive wave vector the situation is reversed. This is expected to result in different coupling efficiencies.

Figure 9 shows that all relative coupling efficiencies display a trend of decaying values for shorter excitation wavelength. In the coupled-wave model for frequencies near the stopgap, situated around $k_x=4.26\times10^{-3}$ nm^{-1}, C_0 increases rapidly with respect to all other C_m. However, in the measurements no pronounced increase in $F_m(k_x)$ is present near the stopgap. We can explain this by taking into account the bandwidth of the wave packets, which is around 30 nm. Because of this large bandwidth, the measured values given for a discrete wave vector will actually constitute an average value over multiple wave vectors. Close to the stopgap, frequencies within the wave packet that are at the red side of the stopgap will leak out of the grating since they are positioned above the lightline. The loss of frequencies results in an effective blueshift of the wave-packet spectrum, which results in a lower measured $F_m(k_x)$.

VII. CONCLUSIONS

We have shown the evolution of individual SPP Bloch harmonics in space and time. The different harmonics, present in one Bloch mode, are separated by Fourier analysis and turn out to have different mode profiles. Also we showed that higher order harmonics couple more efficiently to a near-field probe than lower order harmonics. The $m=-2$ harmonic couples on average 3 orders of magnitude better than the $m=0$ harmonic. This is important to realize because near-field microscopy is the only measurement technique available to study bound, optical Bloch modes. Especially when the amplitude of the different harmonics is used, for example, to determine extremely small variations in the refractive index, one should take into account coupling efficiencies.

ACKNOWLEDGMENTS

This work was made possible by the facilities of the Amsterdam nanoCenter. The work was part of the research program of the Stichting voor Fundamenteel Onderzoek der Materie (FOM), which is financially supported by the Nederlandse organisatie voor Wetenschappelijk Onderzoek (NWO). The support of the EC-funded project PhOREMOST (Grant No. FP6/2003/IST/2-511616) was gratefully acknowledged. This work was also partially supported by NANONED, a nanotechnology program of the Dutch Ministry of Economic Affairs.

*kuipers@amolf.nl

[1] F. Bloch, Z. Phys. **52**, 555 (1928).
[2] P. St. J. Russell, Appl. Phys. B: Photophys. Laser Chem. **39**, 231 (1986).
[3] C. Kittel, *Introduction to Solid State Physics* (Wiley, New York, 1996).
[4] Y. Sugawara, O. B. Wright, and O. Matsuda, Appl. Phys. Lett. **83**, 1340 (2003).
[5] D. M. Profunser, O. B. Wright, and O. Matsuda, Phys. Rev. Lett. **97**, 055502 (2006).
[6] H. Gersen, T. J. Karle, R. J. P. Engelen, W. Bogaerts, J. P. Korterik, N. F. van Hulst, T. F. Krauss, and L. Kuipers, Phys. Rev. Lett. **94**, 123901 (2005).
[7] A. A. Sukhorukov, D. Neshev, W. Krolikowski, and Y. S. Kivshar, Phys. Rev. Lett. **92**, 093901 (2004).
[8] D. Gérard, L. Salomon, F. de Fornel, and A. Zayats, Opt. Express **12**, 3652 (2004).
[9] I. I. Smolyaninov, W. Atia, and C. C. Davis, Phys. Rev. B **59**, 2454 (1999).
[10] M. Lončar, D. Nedeljković, T. P. Pearsall, J. Vučković, A. Scherer, S. Kuchinsky, and D. C. Allan, Appl. Phys. Lett. **80**, 1689 (2002).
[11] M. Martin, T. Benyattou, R. Orobtchouk, A. Talneau, A. Berrier, M. Mulot, and S. Anand, Appl. Phys. B: Lasers Opt. **82**, 9 (2006).
[12] S. I. Bozhevolnyi and L. Kuipers, Semicond. Sci. Technol. **21**, R1 (2006).
[13] S. Jetté-Charbonneau, R. Charbonneau, N. Lahoud, G. Mattiussi, and P. Berini, Opt. Express **13**, 4674 (2005).
[14] H. Raether, *Surface Plasmons* (Springer-Verlag, Berlin, 1986).
[15] E. Ozbay, Science **311**, 189 (2006).
[16] W. L. Barnes, A. Dereux, and T. W. Ebbesen, Nature (London) **424**, 824 (2003).
[17] E. Kretschmann and H. Raether, Z. Naturforsch. A **23**, 2135 (1968).
[18] M. Sandtke, R. J. P. Engelen, H. Schoenmaker, I. Attema, H. Dekker, I. Cerjak, J. P. Korterik, F. B. Segerink, and L. Kuipers, Rev. Sci. Instrum. **79**, 013704 (2008).
[19] M. L. M. Balistreri, J. P. Korterik, L. Kuipers, and N. F. van Hulst, Phys. Rev. Lett. **85**, 294 (2000).
[20] S. I. Bozhevolnyi, B. Vohnsen, and E. A. Bozhevolnaya, Opt. Commun. **172**, 171 (1999).
[21] B. Hecht, H. Bielefeldt, Y. Inouye, D. W. Pohl, and L. Novotny, J. Appl. Phys. **81**, 2492 (1997).
[22] M. Sandtke and L. Kuipers, Nature Photon. **1**, 573 (2007).
[23] R. H. Ritchie, Phys. Rev. **106**, 874 (1957).